doi:10.1016/j.jmb.2006.06.007 J. Mol. Biol. (2006) 361, 140–152

JMB

Available online at www.sciencedirect.com

SCIENCE DIRECT®

ELSEVIER

Xenobiotic Reductase A in the Degradation of Quinoline by *Pseudomonas putida* 86: Physiological Function, Structure and Mechanism of 8-Hydroxycoumarin Reduction

Julia J. Griese[1]†, Roman P. Jakob[1]†, Stephan Schwarzinger[2] and Holger Dobbek[1]*

[1]*Laboratorium Proteinkristallographie Universität Bayreuth Universitätsstrasse 30 95447 Bayreuth, Germany*

[2]*Lehrstuhl Biopolymere Universität Bayreuth, Germany*

A continuous evolutionary pressure of the biotic and abiotic world has led to the development of a diversity of microbial pathways to degrade and biomineralize aromatic and heteroaromatic compounds. The heterogeneity of compounds metabolized by bacteria like *Pseudomonas putida* indicates the large variety of enzymes necessary to catalyse the required reactions. Quinoline, a *N*-heterocyclic aromatic compound, can be degraded by microbes along different pathways. For *P. putida* 86 quinoline degradation by the 8-hydroxycoumarin pathway has been described and several intermediates were identified. To select enzymes catalysing the later stages of the 8-hydroxycoumarin pathway *P. putida* 86 was grown with quinoline. The FMN-containing enzyme xenobiotic reductase A (XenA) was isolated and analysed for its reactivity with intermediates of the 8-hydroxycoumarin pathway. XenA catalyses the NADPH-dependent reduction of 8-hydroxycoumarin and coumarin to produce 8-hydroxy-3,4-dihydrocoumarin and 3,4-dihydrocoumarin, respectively. Crystallographic analysis of XenA alone and in complex with the two substrates revealed insights into the mechanism. XenA shows a dimeric arrangement of two $(\beta/\alpha)_8$ barrel domains each binding one FMN cofactor. High resolution crystal structures of complexes with 8-hydroxycoumarin and coumarin show different modes of binding for these molecules in the active site. While coumarin is ideally positioned for hydride transfer from N-5 of the isoalloxazine ring to C-4 of coumarin, 8-hydroxycoumarin forms a non-productive complex with oxidised XenA. Orientation of 8-hydroxycoumarin in the active site appears to be dependent on the electronic state of the flavin.

We postulate that XenA catalyses the last step of the 8-hydroxycoumarin pathway before the heterocyclic ring is hydrolysed to yield 3-(2,3-dihydroxyphenyl)-propionic acid. As XenA is also found in *P. putida* strains unable to degrade quinoline, it appears to have more than one physiological function and is an example of how enzymes with low substrate specificity can help to explain the variety of degradation pathways possible.

Keywords: xenobiotic reductase; flavin; quinoline; *Pseudomonas putida* 86; Old Yellow Enzyme

*Corresponding author

† J.J.G. and R.P.J. contributed equally to the work.

Present addresses: J.J. Griese, Department of Biomolecular Mechanisms, Max Planck Institute for Medical Research, Germany; R.P. Jakob, Lehrstuhl Biochemie, Universität Bayreuth, Germany.

Abbreviations used: XenA, xenobiotic reductase A; OYE, Old Yellow Enzyme; NG, nitroglycerin; PETN, pentaerythritol tetranitrate.

E-mail address of the corresponding author: holger.dobbek@uni-bayreuth.de

0022-2836/$ - see front matter © 2006 Published by Elsevier Ltd.

Introduction

Approximately 15×10^6 tons of coal tar are produced worldwide every year and are the source for condensed aromatics and *N*-heteroaromatics like quinoline (2,3-benzopyridine).[1] Microorganisms have developed strategies to metabolize naturally occurring aromatic compounds and xenobiotics and as they are able to biomineralize potentially toxic compounds, they can be exploited in the bioremediation of polluted soils and waters.[1] Quinoline is a ubiquitous, soluble, heteroaromatic pollutant with cancerogenic properties.[2] Several bacterial species are capable of degrading quinoline and can grow with quinoline or its derivatives as sole sources of carbon, nitrogen and energy. A unique pathway exists in *Pseudomonas putida* 86 that was isolated from soil near a coal tar factory (Rütgerswerke, Castrop-Rauxel, Germany) by quinoline enrichment culture (Figure 1).[3] Within the 8-hydroxycoumarin pathway of *P. putida* 86 the *N*-heterocyclic ring of quinoline **1** is cleaved preferentially to form 8-hydroxycoumarin **4**. Four intermediates (**2**–**5**) have been identified in the 8-hydroxycoumarin pathway,[2,4] and the enzymes that catalyse the first two steps have been investigated (Figure 1). The molybdo-iron-sulfur flavoprotein quinoline oxidoreductase (QOR) hydroxylates quinoline **1** at C-2 to yield 1*H*-2-oxoquinoline **2**.[5–7] The multicomponent enzyme 1*H*-2-oxoquinoline 8-monooxygenase catalyses the NADH-dependent second hydroxylation reaction at C-8 to yield 1*H*-8-hydroxy-2-oxoquinoline **3**.[8,9] The next two intermediates are 8-hydroxycoumarin **4** and 3-(2,3-dihydroxyphenyl)-propionic acid **5** (Figure 1).[4] The enzymes producing and converting these two compounds are not known. Quinoline degrading *P. putida* strains do not grow with coumarin as a sole source of carbon and energy. However, when bacteria that were grown with quinoline are incubated with coumarin **6**, 3-(2-hydroxyphenyl)-propionic acid **7** accumulates.[4] Characteristic reactions of coumarins are additions to the C-3/C-4 double bond and the nucleophilic opening of the lactone group.[10] Addition of a hydride and a proton to the C-3/C-4 double bond and hydrolysis of the lactone explains the observed products 3-(2,3-dihydroxyphenyl)-propionic acid **5** and 3-(2-hydroxyphenyl)-propionic acid **7** and defines the activity of the enzymes able to convert 8-hydroxycoumarin **4** and coumarin **6** (Figure 1). While 3-(2,3-dihydroxyphenyl)-propionic acid **5** can be further degraded to intermediates of the tricarboxylic acid cycle,[11] 3-(2-hydroxyphenyl)-propionic acid **7** cannot, explaining why *P. putida* 86 does not grow with coumarin as carbon source.[4]

Bacterial enzymes known to catalyse the reduction of the olefinic bond of α,β-unsaturated carbonyl compounds including ketones and esters are a group of enzymes called xenobiotic reductases.[12–18] These enzymes constitute a bacterial subgroup of the Old Yellow Enzyme (OYE) family and are monomeric, homodi- or tetrameric, NAD(P)H-dependent, FMN-containing oxidoreductases with a subunit size of ~40 kDa. Like for OYE itself, the physiological oxidant and with it the physiological function is unknown for almost all members of the OYE family.

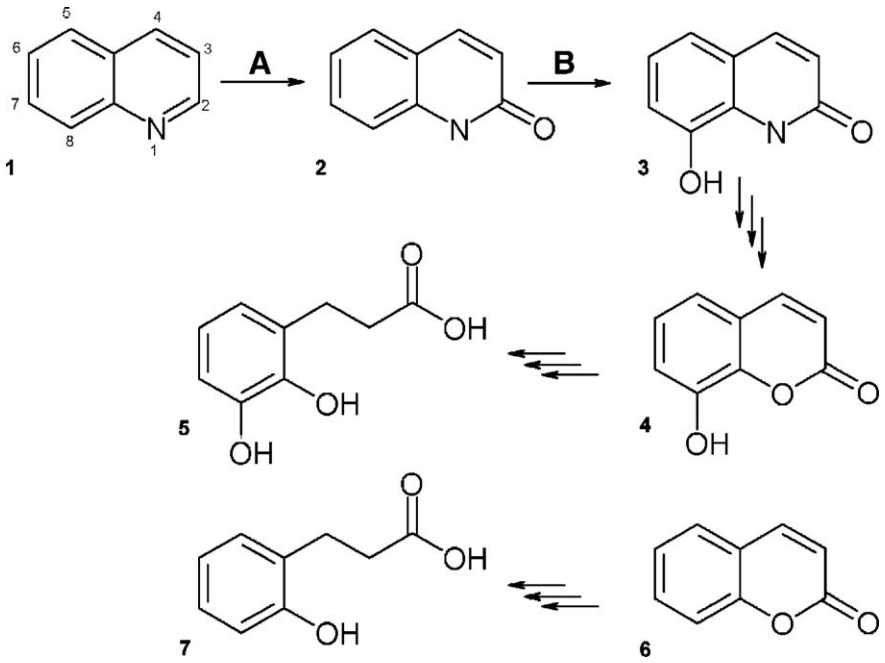

Figure 1. Degradation of quinoline and coumarin by *P. putida* 86. Intermediates of the 8-hydroxycoumarin pathway are depicted.[4] The first reaction of the pathway is labelled with A and is catalysed by quinoline 2-oxidoreductase.[6,7] The second reaction, labelled with B, is catalysed by 2-oxoquinoline 8-monooxygenase.[8,9] Triple arrows indicate that the reaction sequence between the different intermediates is unclear and multiple steps could be involved. In the following the names of all substances depicted are given: (1) quinoline, (2) 1*H*-2-oxoquinoline, (3) 1*H*-8-hydroxy-2-oxoquinoline, (4) 8-hydroxycoumarin, (5) 3-(2,3-dihydroxyphenyl)-propionic acid, (6) coumarin, and (7) 3-(2-hydroxyphenyl)-propionic acid.

Recently, some enzymes of the OYE family were implicated in antioxidant defense by detoxification of reactive electrophilic substrates.[13,19] Xenobiotic reductases catalyse three types of reactions whereby they accept a broad range of electrophilic, xenobiotic compounds: (i) reduction of the olefinic bond of α,β-unsaturated carbonyl compounds like 2-cyclohexenone; (ii) reductive denitration of aliphatic nitro esters like nitroglycerin (NG) or pentaerythritol tetranitrate (PETN); (iii) reduction of nitroaromatic compounds like 2,4,6-trinitrotoluene.

Xenobiotic reductase A (XenA) was originally identified in a *P. putida* strain that had been isolated from NG-contaminated soil.[14] This strain, *P. putida* II-B, grows with NG as sole nitrogen source because XenA denitrates NG. XenA also reduces 2-cyclohexenone to cyclohexanone and the nitro groups of trinitrotoluene to amino groups.[20] XenA is an NADPH-dependent intracellular enzyme with a subunit size of 39.8 kDa (for the apoprotein). It contains one molecule of FMN per subunit. Based on gel filtration chromatography it was suggested to be monomeric in solution.[14]

To investigate the late steps of the 8-hydroxycoumarin pathway, we were searching for enzymes able to convert 8-hydroxycoumarin **4** and coumarin **6**, explaining the reactive principles of the pathway (Figure 1). We found that XenA is expressed in *P. putida* 86 grown with quinoline as sole carbon, nitrogen and energy source. Ligand titration and crystallographic analysis of XenA showed its ability to bind 8-hydroxycoumarin **4** and coumarin **6** in solution and the crystalline state. Kinetic analysis proved its ability to reduce the C-3/C-4 double bond of 8-hydroxycoumarin **4** and coumarin **6**.

Results and Discussion

Expression and purification of XenA

Escherichia coli BL21(DE3) (Stratagene) was used for overexpression of recombinant XenA. Four column chromatography steps were used to purify more than 30 mg XenA with a purity exceeding 95% per 10 g of cells (wet weight). The protein solution was reconstituted with FMN before the gel filtration step because *E. coli* produces XenA to ~70% in the apoform, as approximated by the ratio of absorbance at 280 nm to 464 nm of the protein before and after reconstitution. The reconstituted recombinant protein displayed an absorbance ratio A_{280}/A_{464} of 7.5. The same ratio was determined for XenA purified using the same strategy from *P. putida* 86, indicating that reconstitution with FMN was complete.

Reactivity of XenA

To investigate whether XenA participates in the 8-hydroxycoumarin pathway, its ability to catalyse the reduction of quinoline, coumarin and several of their derivatives with NADPH as a reducing substrate was tested. The previously identified oxidative substrate 2-cyclohexenone was used as positive control.[20] Quinoline, 2-quinolinol, 4-quinolinol and 2,8-quinolinediol did not oxidise reduced XenA (data not shown). Coumarin and 8-hydroxycoumarin were reduced by XenA, albeit more than tenfold slower than 2-cyclohexenone. XenA has an apparent turnover number of 8 s^{-1} with 2-cyclohexenone, 0.4 s^{-1} with coumarin and 0.2 s^{-1} with 8-hydroxycoumarin (Table 1). XenA shows an ~fourfold preference for NADPH over NADH. It will also reduce molecular oxygen with a specific activity of 0.2 unit/mg at oxygen saturation of the buffer (263 μM at 25 °C, 1 bar). Therefore, assays were conducted under anaerobic conditions. Apparent values for the Michaelis constant (K_M) for all three substrates are in the same range with 33(±4) μM for 2-cyclohexenone, 23(±2) μM for coumarin and 34(±3) μM for 8-hydroxycoumarin. The apparent K_M value for NADPH, determined with 2-cyclohexenone as oxidative substrate is 61(±7) μM (Table 1).

Real-time NMR spectra were recorded to determine the products of the reactions with 8-hydroxycoumarin and coumarin (Figure 2). For comparison, reference spectra of educts (8-hydroxycoumarin, coumarin, and NADPH) and possible products (3,4-dihydrocoumarin, 3-(2-hydroxyphenyl)-propionic acid and $NADP^+$) were measured. The newly appearing resonances agreed well with the formation of 8-hydroxy-3,4-dihydrocoumarin and 3,4-dihydrocoumarin, respectively, and $NADP^+$, while the resonances disappearing corresponded to 8-hydroxycoumarin and coumarin, respectively, and NADPH. Approximate rate constants derived for the time-dependent evolution of selected resonances show similar rates for $NADP^+$ and 8-hydroxy-3,4-dihydrocoumarin production and for NADPH and 8-hydroxycoumarin decay (data not shown). The nearly complete decay of resonances of the educts shows that the equilibria of both reactions (8-hydroxycoumarin and coumarin) are on the side of products (Figure 2). No resonances indicating a hydrolysis of the lactone group were detectable during the 5 h of the real time NMR experiment.

Table 1. Steady-state kinetic properties of xenobiotic reductase A

Substrate	Spec. act. (units/mg)	K_M (μM)	k_{cat} (s^{-1})	k_{cat}/K_M ($\mu M^{-1} s^{-1}$)
2-Cyclohexenone[a,c]	9	33±4	8±1	0.24
8-Hydroxycoumarin[a,d]	0.4	34±3	0.2	0.01
Coumarin[a,d]	0.8	23±2	0.4	0.02
NADPH[b,c]	9	61±7	8±1	0.13

Apparent kinetic constants were derived from steady-state kinetic analyses. The assays were performed at 25 °C in 1 ml of 50 mM potassium phosphate buffer (pH 7.0). The compounds 7-hydroxycoumarin, quinoline, 2-quinolinol, 4-quinolinol, 2,8-quinolinediol, 2,4-dinitrophenol, picric acid and metronidazole were also tested, but no activity was detected.

[a] Reductive substrate: 150 μM NADPH.
[b] Oxidative substrate: 300 μM 2-cyclohexenone.
[c] The reaction mixture contained 250 nM XenA.
[d] The reaction mixture contained 1 μM XenA and 1% DMSO.

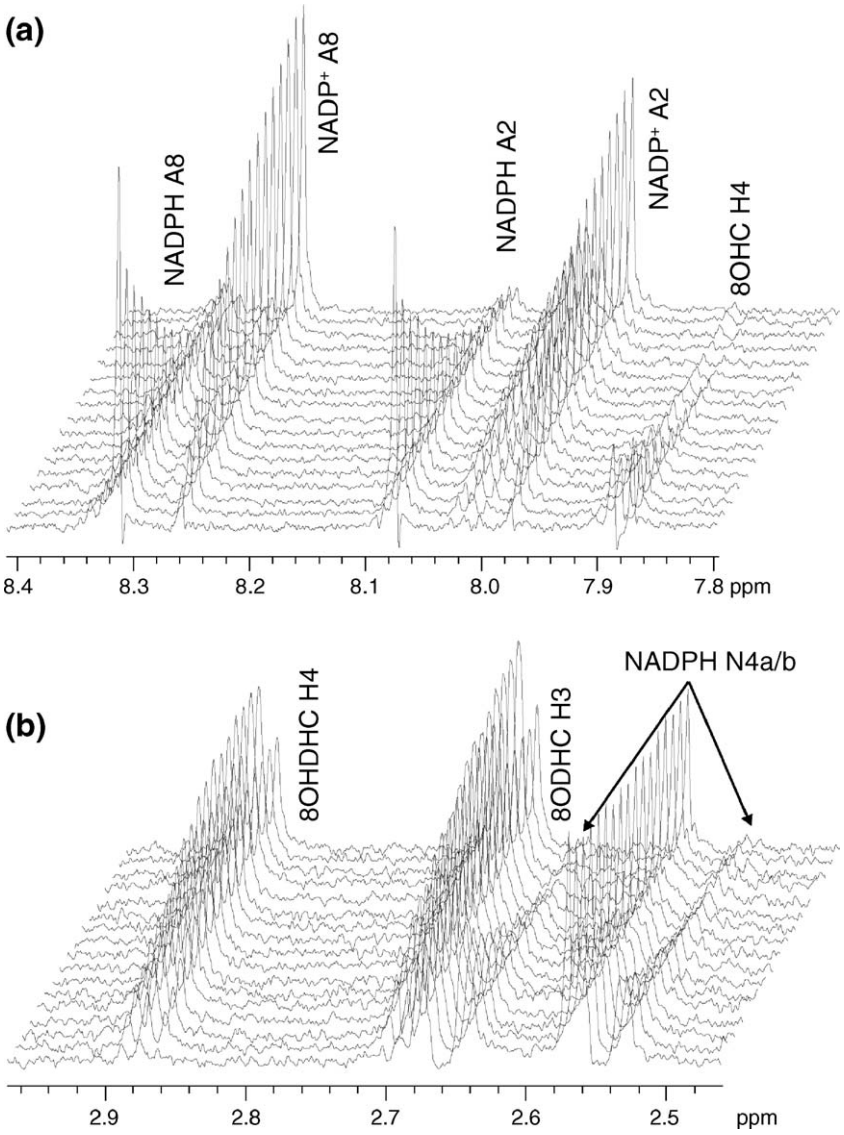

Figure 2. Kinetic analysis of XenA substrate turnover by real-time NMR spectroscopy. Series of 1D proton NMR spectra recorded at 600 MHz. The time between each spectrum shown is approximately 18 min. The last spectrum shown was recorded 288 min after addition of XenA. (a) A portion of the spectra showing the decrease and increase of the signals corresponding to the adenosine protons A8 and A2 of NADPH and $NADP^+$, respectively. A2 of $NADP^+$ overlaps with the increasing signal of the nicotinamide resonance N5 of $NADP^+$ (label omitted for clarity). The decaying doublet at 7.88 ppm corresponds to H4 of the substrate 8-hydroxycoumarin (8OHC). (b) The increasing signal of protons H3 (2.69 ppm) H4 (2.88 ppm) of the enzymatic product, 8-hydroxy-3,4-dihydrocoumarin (8OHDHC). H3 partially overlaps with the decaying signal of the protons at position 4a of the nicotinamide moiety of NADPH (4a: 2.66 and 4b: 2.55 ppm, respectively). The positions of H3 and H4 are almost exactly identical to those of 3,4-dihydrocoumarin but different from the hydrolysed form, clearly suggesting that 8-hydroxy-3,4-dihydrocoumarin is the end product of the enzymatic reaction of XenA. The reaction with coumarin yields essentially identical results, except that enzymatic turnover is approximately two to threefold higher (data not shown).

Ligand binding

The titration of oxidised XenA with coumarin and 8-hydroxycoumarin resulted in perturbations of the electronic absorption spectrum of the enzyme-bound FMN and allowed determination of the dissociation constant of the complexes (Figure 3). Optical titration with the two substrates showed isosbestic points at 502 nm for 8-hydroxycoumarin (Figure 3(a)) and 496 nm for coumarin (Figure 3(c)). The absorption changes recorded upon titration of oxidised XenA with 8-hydroxycoumarin (Figure 3) are characteristic of charge transfer complexes between ligands with a deprotonated phenolic hydroxyl group and the oxidised flavin.[21] The spectra display a hypochromic effect at 464 nm, corresponding to the flavin absorption maximum, and a hyperchromic effect at 600 nm probably elicited by the charge transfer interaction. Coumarin causes only a perturbation of the electronic absorption spectrum of FMN without additional charge transfer interactions (Figure 3(c)), as found for titrations of OYE with ligands that do not contain a phenolic group.[21] There is no hyperchromic effect around 600 nm, and the hypochromic effect at 464 nm is accompanied by a red shift of the entire flavin absorbance (Figure 3(c)). Plots of absorption change at 464 nm *versus* ligand concentration and fitting to equation (1) gave dissociation constants (K_d) of 2.5(±0.5) μM and 5.0(±1.8) μM for 8-hydroxycoumarin and coumarin, respectively (Figure 3(b) and (d)).

Overall structure and oligomerisation state

The structure of native oxidised XenA from *P. putida* 86 was solved by single isomorphous replacement combined with anomalous dispersion of an iodide derivative (Table 2). The resulting electron density was basically interpretable and displayed the overall fold of the $(\beta/\alpha)_8$-barrel. To optimize automatic model building by using different phase sources, a Patterson search was carried out with a search model constructed from the crystal structure of morphinone reductase (PDB-ID:1GWJ).[22] The combined phases from SIRAS

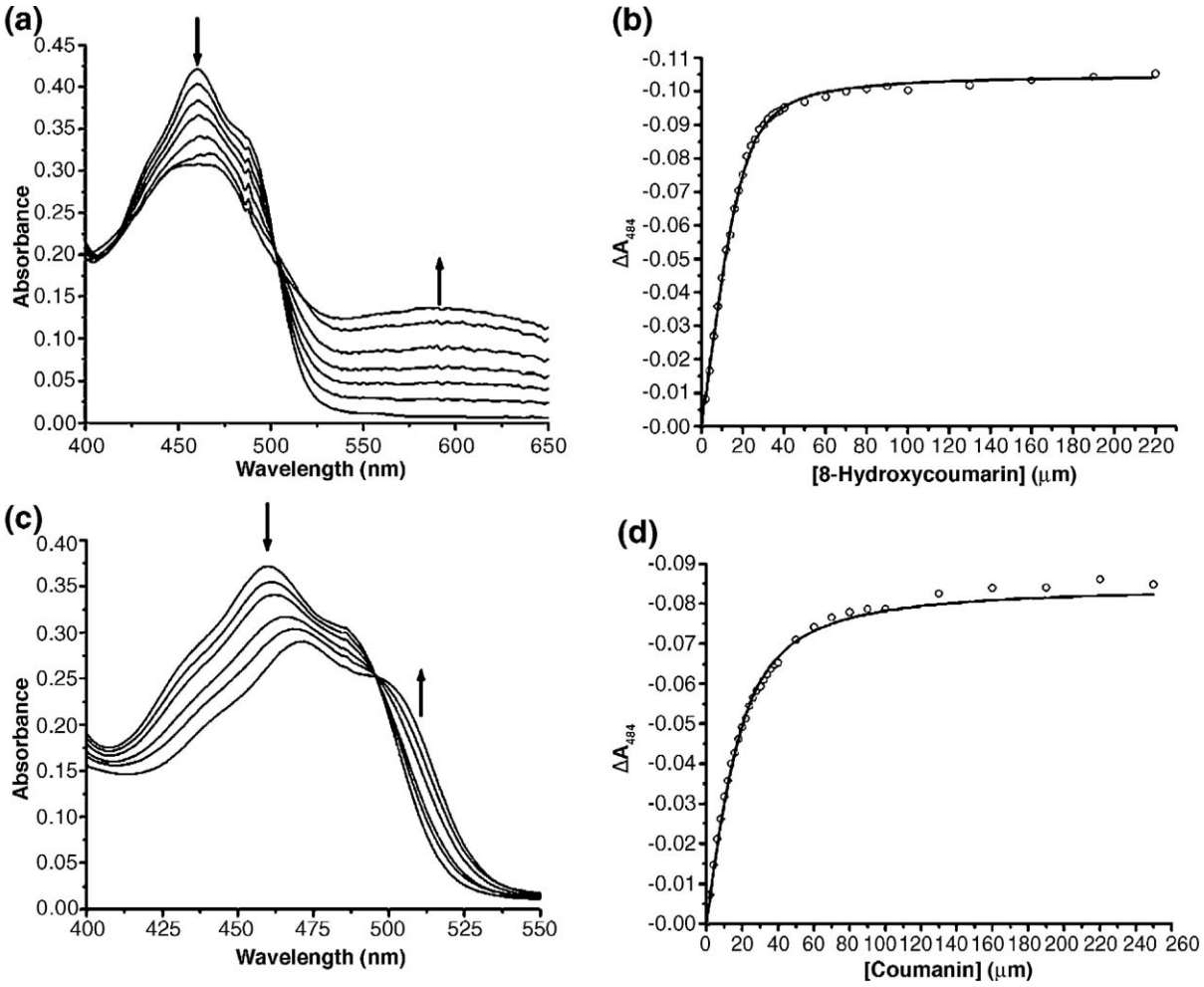

Figure 3. Titrations of XenA with 8-hydroxycoumarin and coumarin. Conditions: 30 μM XenA in 50 mM potassium phosphate buffer (pH 7.0), 20 °C. (a) Spectral changes recorded on titrating XenA with 8-hydroxycoumarin. For clarity, only selected spectra are shown, including the spectra of start and end points of the titration. (b) Plot of absorbance change at 464 nm *versus* 8-hydroxycoumarin concentration. The continuous line results from the fit to equation (1). (c) and (d) As for (a) and (b), but for titration of XenA with coumarin. Arrows indicate the direction of spectral changes.

phasing and the molecular replacement solution allowed automatic tracing and model building including the majority of the water structure. The structure was refined to 1.5 Å resolution with a final *R*-factor of 18.2% (Table 3). Stereochemical parameters of the model are good except for one residue, Trp302, which is found in the disallowed region of the Ramachandran plot (Table 3). The XenA monomer adopts a $(\beta/\alpha)_8$-barrel fold where eight α-helices surround eight twisted β-strands, forming a cylindrical structure (Figure 4(a)). On the N-terminal side of the β-strands, the barrel is closed by a β-hairpin, whereas on the C-terminal side it is wide open. The flavin is bound at the C-terminal end. The longer C-terminal loops contain additional secondary structure elements, namely several short 3_{10}-helices, α-helices and two short β-strands (Figure 4(b); the C-terminal loops are numbered

Table 2. Phasing statistics

	Space group	Unique/ observed refl.	R_s[b] (Overall/ last shell)	Resolution (Å) (Overall/ last shell)	Completeness (%) (Overall/ last shell)	$(I)/(\sigma I)$ (Overall/ last shell)	Phasing power. (Centric/Acentric -Iso/-Ano/)	R_{Cullis}[c] (Acentric- Iso/-Ano)	FOM (Centric/ acentric)
Native	*I*222	115,072/ 268,137	0.036/0.187	20–1.50/ 1.60–1.50	97.9/90.5	16.2/5.2			
KI[a]	*I*222	33,324/ 79,024	0.059/0.155	20–2.25/ 2.35–2.25	94.3/95.0	12.8/6.1	0.67/0.65/0.93	0.88/0.84	0.25/0.23

Friedel mates were treated as independent reflections.
[a] Heavy atom derivative: 12 iodide sites per a.u.
[b] $R_s = \Sigma_h \Sigma_i |I_i(h) - \langle I(h) \rangle| / \Sigma_h \Sigma_i I_i(h)$; where *i* are the independent observations of reflection *h*.
[c] $R_{Cullis} = \Sigma_h (||F_{PH}(h) - F_P(h)| - |F_{Hcalc}(h)||) / \Sigma_h |F_{PH}(h) - F_P(h)|$.

Table 3. Crystallographic data and refinement

Data set	XenA	XenA$^{8\text{-OH-Cum}}$	XenA^{Cum}
Total/unique refl.	268,181/60,235	222,082/67,580	196,693/67,020
R_s[a]	0.042 (0.204)	0.059 (0.239)	0.060 (0.204)
Resolution (Å)	20–1.50 (1.6–1.5)	20–1.42 (1.50–1.42)	20–1.42 (1.50–1.42)
Completeness (%)	98.5 (92.6)	94.9 (85.5)	93.9 (79.8)
$(I)/(\sigma I)$	22.0 (7.2)	12.6 (4.9)	11.4 (4.9)
Model R/R_{free}-factor (%)[b]	18.2/19.1	18.9/20.2	19.1/20.6
rms deviation from ideal geometry			
Bonds (Å)	0.0082	0.0083	0.0082
Angles (°)	1.27	1.29	1.29
Ramachandran statistics (%)	90.5/8.6/0.7/0.3	88.5/10.5/0.7/0.3	90.5/8.5/0.7/0.3
Most favoured/additional/ generously allowed/disallowed regions			

Friedel mates were merged. XenA: XenA crystal with sulphate ion in the active site. XenA$^{8\text{-OH-Cum}}$: crystal of XenA soaked with 8-hydroxycoumarin. XenA^{Cum}: crystal of XenA soaked with coumarin. All three crystals belonged to space group *I*222. The values given in parantheses are for the highest resolution shell. The Ramachandran statistics were calculated with PROCHECK.[50]

[a] $R_s = \Sigma_h \Sigma_i | I_i(h) - \langle I(h) \rangle | / \Sigma_h \Sigma_i I_i(h)$; where i are the independent observations of reflection h.

[b] The free R-factor was calculated from 5% of the data, which were removed at random before the structure was refined.

according to the preceding β-strands). Loop L3 is the longest loop, consisting of 48 residues, and contains most of the barrel's extra secondary structure elements and active site residues.

Like many other OYE family members, XenA forms a homodimer. Monomer A in the asymmetric unit is related to monomer B by a crystallographic 2-fold axis, resulting in approximately opposite directions for the barrel openings. The crystallographic 2-fold axis forming the dimer runs between helices α1 of the two subunits. Additional interactions between the monomers are built up by the C terminus from helix αF to αH. Trp358 in helix αH protrudes into the active site of the neighbouring monomer and forms part of its FMN and substrate binding pocket (see below). The dimer interface shields 10% of the monomer surface (1380 Å^2 per monomer). It lies on the opposite side of the barrel in comparison to the dimer interface of OYE that is formed by helices 4, 5, and 6.[23]

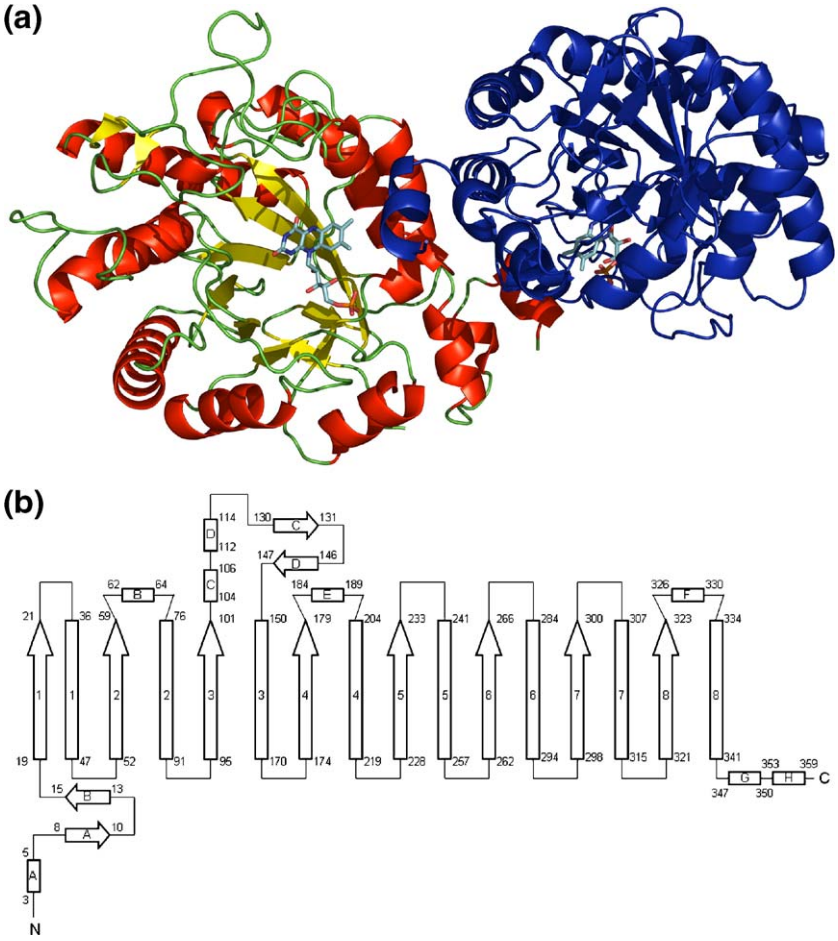

Figure 4. Overall structure of XenA. (a) Ribbon diagram of the XenA dimer. Monomer A is coloured according to its secondary structure: red, helices; yellow, β-strands; green, coils. Monomer B is coloured blue. The FMN cofactors of both monomers are shown in stick form with carbon in cyan, nitrogen in blue, oxygen in red, and phosphorus in orange. (b) Topology of XenA. Helices are displayed as rectangles, strands as arrows. Helices and strands of the barrel are numbered according to their order in the barrel. Extra barrel secondary structure elements are designated by letters. The numbers at the beginning and end of each secondary structure element account for the amino acid number.

The structure of XenA is highly similar to that of other OYE homologues. The closest homologue of XenA is the flavoprotein YqjM from *Bacillus subtilis*.[13,24] The two proteins share an overall amino acid sequence identity of 40% and similarity of 54% and are closely related in structure: 292 residues can be superimposed with a root mean square deviation of 1.2 Å.[25] The major structural difference in the monomers is in loop L3, which consists of 48 residues in XenA, whereas loop L3 of YqjM consists of only 30 residues. YqjM has been described as a dimer of dimers, while XenA is a homodimer in the crystal. In place of the active site residue Trp358 of XenA, YqjM has an arginine finger protruding into the adjacent active site.[24] Based on sequence comparisons of the OYE homologue YqjM from *B. subtilis* with other OYE family members, a new bacterial subgroup of the OYE family has been suggested.[24] However, several C-terminal residues of YqjM suggested to be invariant in this bacterial subgroup are not found in XenA from *P. putida* 86, the closest relative of YqjM.[24] Specifically, Arg312, Gln333, and Arg336 of YqjM align with Ala330, Pro354 and His357 of XenA, respectively. Arg336 is the residue that extends into the adjacent active site of YqjM. In XenA, this residue is functionally replaced by Trp358, resulting in a comparable active site composition from two monomers. However, other distinctive features of the proposed new subgroup of the OYE family are found in XenA as well, such as Cys25 and Tyr27, which are conserved in this subgroup, but not in the OYE family.[24]

The FMN binding site

A pocket leading to the active site is wide open with an average diameter of around 18 Å measured between the Cβ-atoms of the surrounding amino acids. It is formed between the two monomers and has at its bottom the FMN cofactor in an elongated conformation (Figure 4). The FMN cofactor is bound at the C-terminal end of the β-barrel, above β-strands 1 and 8, with its *si* face exposed to the solvent. The protein matrix interacts with the pyrimidine ring and the ribityl side-chain of the flavin through hydrogen bonds. Most of the interactions between apoprotein and flavin are conserved within the OYE family, for example a glutamine residue (Gln99), a histidine pair (His178 and His181), and an arginine residue (Arg231) bind N-3, O-2 and N-1 of the cofactor, respectively. O-4 of the FMN is bound by the amide proton of Ala57 and the γ-sulfhydryl group of Cys25. The amide proton of Cys25 binds N-5. OYE and most of its characterised homologues contain a threonine residue in a position equivalent to Cys25 (Thr37 in OYE), reported to increase the redox potential of the cofactor by stabilising the negative charge of the reduced flavin through hydrogen bonding with O-4.[26] Based on structural comparisons, the same function can be assigned to Cys25 of XenA. For instance, the corresponding cysteine residue in YqjM adopts different conformations depending on the occupation of the active site: in the absence of a ligand, three different conformations were discernible in the electron density, whereas in the presence of a ligand, the γ-sulfhydryl group pointed exclusively to O-4 of the flavin. It was suggested that this residue modulates the redox potential of the flavin depending on the presence of substrates.[24] However, in XenA, Cys25 is in hydrogen-bonding distance to O-4 of the cofactor in all three structures, indicating a role of Cys25 independent of the occupation of the active site.

The dimethylbenzene ring of flavin is stabilised by hydrophobic interactions with Met24 on its *re* side and Trp358 of the other monomer on the *si* side. Trp358 extends into the active site of the adjacent monomer and closes it on the side of the dimethylbenzene moiety of the cofactor through a face-on-edge π−π interaction (Figure 5). The terminal phosphate group is embedded into an electropositive groove of the protein formed by loops L7 and L8 and the positive end of the macrodipole of helix αF.

Ligand complexes in the active site of XenA

The crystal structure of XenA has been analysed in complex with sulphate and the substrates coumarin and 8-hydroxycoumarin.

The active site structure of oxidised, uncomplexed XenA is shown in Figure 5. An anion binds above the oxidised flavin as found for other members of the OYE family.[23,24,27] A sulphate molecule could be modelled in the electron density. The sulphate ion is in hydrogen-bonding distance to His178, His181, and Tyr183 (Figure 5).

The coumarin complex is stabilized by π−π stacking interactions between coumarin and the isoalloxazine ring (Figure 6(b)). The carbonyl

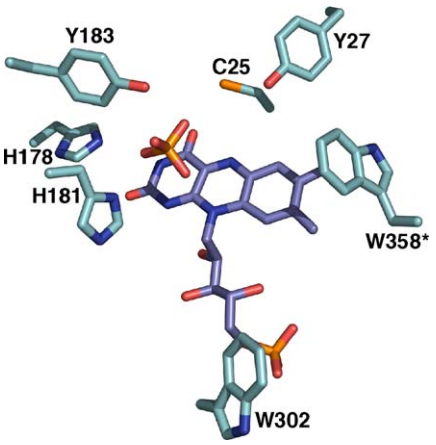

Figure 5. Active site of oxidised XenA in complex with sulphate. All residues are displayed in stick mode with carbon atoms of the apoprotein in cyan, carbon atoms of the flavin in violet, nitrogen in blue, oxygen in red, and phosphorus and sulphur in orange. The asterisk denotes a residue from monomer B.

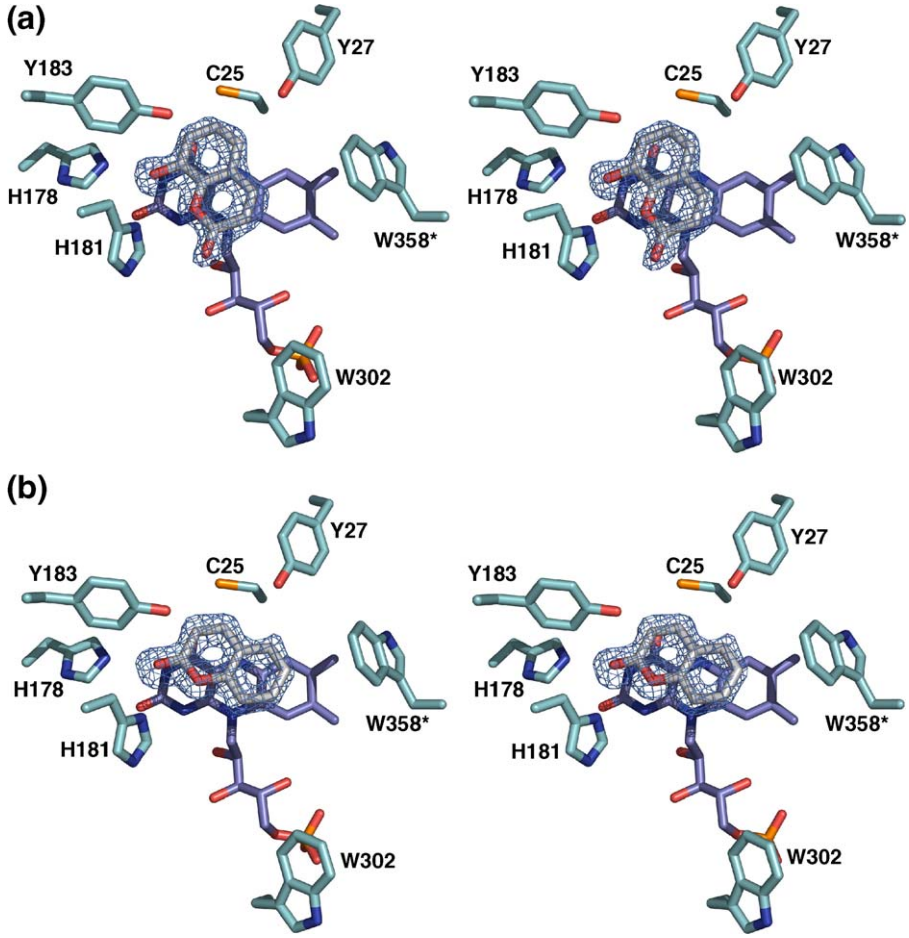

Figure 6. Stereo view of the active site of XenA in complex with (a) 8-hydroxycoumarin, (b) coumarin. All residues are displayed in stick mode with carbon atoms of the apoprotein in cyan, carbon atoms of the flavin in violet, carbon atoms of the ligand in grey, nitrogen in blue, oxygen in red, and phosphorus in orange. Initial F_o–F_c electron density maps for the ligands are contoured at 3 σ.

oxygen of coumarin is in hydrogen-bonding distance to His178 and His181. His181 also binds O-1 of the coumarin. There are no further interactions with the protein. Notably, Tyr27 does not contribute to substrate binding. The corresponding residue in YqjM and the C-terminal tyrosine residue Tyr375 that occupies the corresponding position in OYE have been shown to coordinate the carbonyl oxygen atom of the inhibitor *p*-hydroxybenzaldehyde, leading to the assumption that this tyrosine residue contributes to substrate specifity. In XenA, the histidine pair His178 and His181 appears to be exclusively responsible for substrate specificity and orientation by hydrogen-bonding in the active site. Through coordination of the carbonyl oxygen of an α,β-unsaturated carbonyl substrate like coumarin by the histidine pair, the reactive olefinic bond is positioned optimally for proton and hydride transfer and becomes polarised, activating the β-carbon for nucleophilic attack: C-4 (the β-carbon) of coumarin is in 3.7 Å distance to the hydride donor, N-5 of the FMN cofactor, whereas C-3 (the α-carbon) is close to Tyr183, the presumptive proton donor. This observation fits the catalytic mechanism that has been proposed for OYE with a hydride transfer from the flavin N-5 to the β-carbon, followed by proton transfer from the active site acid Tyr196 to the α-carbon of α,β-unsaturated carbonyl substrates.[19,28,29] However, mutational studies of PETN reductase have shown that the corresponding tyrosine residue of this OYE homologue is not essential for catalysis,[30] while morphinone reductase contains a cysteine residue in place of Tyr196 of OYE, which is not the essential active site acid.[22] For PETN reductase and morphinone reductase, it was suggested that the proton is transferred from the solvent to the substrate.[30,31] The studies on PETN reductase and morphinone reductase show that, despite a conserved active site architecture, the function of individual residues may not be conserved and has to be investigated for each enzyme individually. Furthermore, a dependence on the type of substrate cannot be ruled out. Reactivity analysis of XenA mutations will have to reveal if Tyr183 is essential for protonation of the substrate.

In contrast to coumarin, 8-hydroxycoumarin binds in the active site in a fashion that does not allow hydride transfer from flavin N-5 to C-4 of 8-hydroxycoumarin, as the two atoms are 4.7 Å apart (Figure 6(a)). 8-Hydroxycoumarin is flipped by 180° around the central C-1a – C-4a axis in comparison to coumarin, so that the phenolic hydroxyl group at C-8 is hydrogen bonded to the histidine pair. His181 also coordinates O-1. The ligand thus does not bind parallel to the long axis of the isoalloxazine ring like coumarin, but is rotated by ~45° relative to this axis. Again, there are no further interactions with the protein except those mediated by the histidine pair and the flavin. It has been proposed that phenolic compounds bind to oxidised OYE in the deprotonated state, forming a charge transfer complex with the flavin with characteristic absorbance.[21] These typical absorption changes have been seen upon titration of oxidised XenA with 8-hydroxycoumarin and make it likely that it binds in the deprotonated phenolate state to oxidised XenA. As the phenolate group is able to form stronger hydrogen bonds with the histidine pair than the carbonyl oxygen the deprotonation would explain why the binding modes of 8-hydroxycoumarin and coumarin differ so remarkably. The binding mode of 8-hydroxycoumarin appears to be non-productive, as the reactive olefinic bond of 8-hydroxycoumarin does not lie above the flavin N-5 or in close proximity to Tyr183. Due to steric clashes, it is unlikely that re-orientation of the substrate in the active site is possible. Thus, substrate bound in the unproductive mode would have to be released before binding in the productive mode would be possible. The presence of a dominant non-productive binding mode would be expected to result in substantially lower apparent K_M and k_{cat} values for 8-hydroxycoumarin compared to coumarin. However, both ligands show comparable apparent K_M and k_{cat} values (Table 1), arguing for similar binding geometries in the reduced enzyme. A different binding geometry of 8-hydroxycoumarin in the reduced enzyme could originate from an influence of the electron distribution and delocalization of the isoalloxazine ring on the pK_a value of the phenol hydroxyl group of 8-hydroxycoumarin. While oxidised FMN can stabilise the phenolate anion by charge transfer interactions, thereby effectively lowering the pK_a of the phenol, $FMNH_2$ will do so to a much smaller extent. It appears likely that in oxidised XenA 8-hydroxycoumarin binds in the phenolate form while in the reduced state the phenol would be more stable. As the orientation of the ligands in the active site is dominated by the strength of the hydrogen bonding interaction with the donating histidine pair, the deprotonated form would bind preferentially with the phenolate oxygen while the protonated 8-hydroxycoumarin would bind with the carbonyl oxygen of the lactone group to the histidine pair. The consequence would be the prevalence of a productive binding mode of 8-hydroxycoumarin in reduced XenA, which is in agreement with the apparent kinetic constants and the product detected by NMR experiments (Figure 2). Non-productive binding modes in the oxidised states have also been found for ligand complexes of the related flavoproteins PETN reductase[27] and nitroreductase.[32] It has been suggested that changes in charge distribution upon reduction of the flavin could help to prevent some molecules from binding in flavoproteins with broad substrate specificity, like nitroreductases and xenobiotic reductases.[32]

Single crystal absorption spectra of uncomplexed and complexed XenA are comparable to the solution spectra, and we can conclude that ligand binding in solution and in the crystalline state are equivalent (data not shown).

Physiological role of XenA

Evidence has been obtained that XenA can participate in the 8-hydroxycoumarin pathway of *P. putida* 86. XenA is expressed in *P. putida* 86 when grown with quinoline as a sole source of carbon, nitrogen and energy, and it catalyses the NADPH-dependent reduction of 8-hydroxycoumarin, a known intermediate in the degradation of quinoline by *P. putida* 86.[2] Chemical reactivity of coumarin and its derivatives, our NMR analysis of the products formed and the orientation of coumarin in the active site complex argue that the C-3/C-4 double bond of 8-hydroxycoumarin is reduced by XenA to yield 8-hydroxy-3,4-dihydrocoumarin. Additionally, the conversion of coumarin by *P. putida* 86 is explained by our kinetic analysis of XenA with coumarin as an oxidising substrate yielding 3,4-dihydrocoumarin, which, when subsequently hydrolysed, produces 2-hydroxyphenylpropionic acid, which was found to accumulate in *P. putida* 86. NMR clearly shows that XenA only catalyses reduction of the C-3/C-4 double bond, but not the hydrolysis of the lactone.

XenA appears to have several distinct biological functions in addition to its participation in the degradation of quinoline, as it is also found in the genome sequence of *P. putida* KT2440 that does not contain the genes for other enzymes of the 8-hydroxycoumarin pathway. Furthermore, XenA is also highly expressed in *P. putida* II-B grown in the absence of coumarins, constituting ~14% of the total soluble protein.[14] The broad substrate specificity of XenA makes it an ideal candidate for participation in the degradation of several heteroaromatic and potentially toxic compounds. Enzymes with such a broad substrate specificity can to some extent explain the wide variety of aromatic, and often xenobiotic, substances that are degraded by bacteria like *P. putida* 86. Remarkably, XenA is to our knowledge the first OYE homologue implicated in the *in vivo* degradation of heteroaromatic compounds.

Materials and Methods

Chemicals

All chemicals used were of analytical grade. Coumarin and 2-cyclohexenone were obtained from Fluka. 8-Hydroxycoumarin was prepared essentially as described by Cerqueira *et al.*[33] All chromatography materials were from Amersham Biosciences.

Growth of *P. putida* 86

P. putida 86 was cultured aerobically in 35 l fermentors at 30 °C in a quinoline minimal medium.[34] Whenever quinoline and 2-oxoquinoline were undetectable in the fermentation broth, further portions of quinoline (0.5 ml/l) were added. At an optical density (600 nm) of approximately 3.5, cells were harvested by centrifugation, frozen in liquid nitrogen, and stored at −30 °C until further use.

PCR, cloning, sequencing and expression

The nucleotide sequence of *xenA* from *P. putida* KT2440 was obtained from GenBank (accession no. AF154061). The open reading frame of *P. putida* 86 *xenA* was amplified by polymerase chain reaction, using a *P. putida* 86 colony as template, and cloned into pET-11a (Novagen). The construct was verified by sequence analysis and was transformed into *E. coli* BL21(DE3) (Stratagene) for expression. *E. coli* strain BL21(DE3) harbouring plasmid pET-11a with the insertion of *xenA* was grown aerobically at 25 °C in 4 l of LB medium containing 100 μg/ml ampicillin after 1% inoculation. Expression was induced with 0.1 mM IPTG at an optical density (600 nm) of ~0.7. Cells were harvested by centrifugation 18 h after induction, frozen in liquid nitrogen, and stored at −30 °C until further use.

Purification of XenA

The enzyme heterologously expressed in *E. coli* BL21 (DE3) was purified by four column chromatography steps: anion exchange chromatography, hydrophobic interaction chromatography, gel filtration and a second anion exchange chromatography. All chromatography steps were carried out at 16 °C; in between the protein solution was kept on ice. After the hydrophobic interaction chromatography step XenA-containing fractions were incubated with 5 mM FMN on ice over night.

From *P. putida* 86, XenA was purified in essentially the same way, except that the protein was not reconstituted with FMN.

Determination of protein concentration

The concentration of XenA holoprotein was determined using a millimolar extinction coefficient of 12.2 $mM^{-1}cm^{-1}$ at 464 nm. The extinction coefficient of XenA-bound FMN was evaluated as follows: a spectrum of the native protein was recorded. The protein was then denatured by the addition of 0.1 vol. 50% trichloroacetic acid, and the precipitated protein removed by centrifugation. The supernatant was neutralised with solid sodium bicarbonate and the spectrum recorded against a reagent blank without XenA. The extinction coefficient of XenA-bound FMN at its absorption maximum (464 nm) was calculated from the known extinction coefficient of 12.2 $mM^{-1}cm^{-1}$ at 450 nm for free FMN.[35]

Substrate specificity

Apparent steady-state kinetic constants were recorded by following the oxidation of NADPH at 340 nm in a Specord 30 spectrophotometer (Analytik Jena) while systematically varying the substrate concentration. Reactions were initiated by addition of enzyme and monitored for 2 min. All experiments were conducted three times and results were averaged. One unit of enzyme activity was defined as the oxidation of 1 μmol NADPH per min at 25 °C in the assay buffer.

The reaction mixture was made anaerobic by flushing with nitrogen. Enzyme assays were measured at 25 °C in 1 ml of 50 mM potassium phosphate buffer (pH 7.0), containing 150 μM NADPH, and 250 nM XenA, where 2-cyclohexenone was used as oxidative substrate, or 1 μM XenA, where coumarin or 8-hydroxycoumarin were used as oxidative substrate. Apparent steady-state kinetic constants for NADPH were determined with 300 μM 2-cyclohexenone as oxidative substrate. 8-Hydroxycoumarin and coumarin were dissolved at 100-fold concentration in dimethyl sulphoxide (DMSO), keeping the DMSO concentration in the reaction mixture constant at 1%. The software GraFit version 5.0.10 (Erithacus Software Limited) was used for evaluation of the data.

NMR spectroscopy

1D-proton NMR spectra of the individual substances (coumarin, 8-hydroxycoumarin, 3,4-dihydroxycoumarin, 3-(2-hydroxyphenyl)-propionic acid, NADPH, and $NADP^+$) in an aqueous buffer (pH 7.0), containing 50 mM potassium phosphate and 5% ^2H_2O were measured on a Bruker Avance 400 spectrometer equipped with a HCN-triple-resonance probe head with *z*-axis gradients at 293 K. The residual water signal was suppressed using double-pulsed field gradient echo technique.[36] The concentration of each substance was 100 μM. 256 transients with 16.384 complex data points were recorded and zero-filled to 64,000 data points prior to Fourier transformation. Signal assignments for NADPH, $NADP^+$, and coumarin were taken from the literature.[37–39] Assignments for the other compounds were derived from 2D-NOESY[40] spectra and interpretation of 1D-spectra. 2D-NOESY experiments with a mixing time of 800 ms and with double-pulsed field gradient echos for solvent suppression[36] were recorded at 600 MHz with 4000 complex data points in the direct dimension and 256 data points in the indirect dimension. The assignments were used to identify compounds in the reaction mixture during kinetic experiments (data not shown).

Kinetic NMR experiments of the turnover of coumarin and 8-hydroxycoumarin by XenA were recorded on a Bruker DRX 600 spectrometer equipped with a HCN-triple resonance probe head with *x,y,z*-axis gradients at 288 K. The concentration of the substrate was 100 μM and 150 μM the cofactor NADPH in each case. After the first data point enzyme was directly added into the NMR-sample tube to a final concentration of 0.8 μM. The dead time for mixing and

equilibration was approximately 5 min. A series of 50 experiments with 128 transients was recorded, each experiment requiring approximately 6 min. Spectra were evaluated with MESTREC 2.3a.[41] The time-dependent intensities of selected signals were fit using Microcal™ Origin® version 6.0 (Microcal Software, Inc.) assuming exponential decay/build up to extract approximate rates. All chemical shifts were referenced relative to internal TSP.

Ligand binding titrations

30 μM oxidised XenA in 50 mM potassium phosphate buffer (pH 7.0), at 20 °C, was titrated by systematically varying the ligand concentration. Spectra were recorded between 240 and 650 nm with a 8452 A diode array spectrophotometer (Hewlett Packard). Spectral changes evoked by the addition of ligand to XenA agree with a 1:1 binding stoichiometry, and the isosbestic points during the titration are attestive of a single step process. Absorption changes at two selected wavelengths with the largest spectral perturbations were plotted against ligand concentration. The data were fitted with the software Microcal™ Origin® version 6.0 (Microcal Software, Inc.) to the quadratic function (equation (1)) to calculate the dissociation constant (K_d) for the enzyme–ligand complex:

$$\Delta A = \frac{\Delta A_{max}}{2E_T} \times \left[(L_T + E_T + K_d) - \left((L_T + E_T + K_d)^2 - (4L_T E_T) \right)^{0.5} \right] \quad (1)$$

where ΔA_{max} is the maximum absorption change at the selected wavelength, L_T is the total ligand concentration, and E_T is the total enzyme concentration.

Protein crystallisation and structure determination

XenA was crystallised by vapour diffusion using the hanging-drop setup at 16 °C. The reservoir solution (500 μl) contained 1.4 – 1.7 M ammonium sulphate in 0.1 M Hepes buffer (pH 7.5). Two drops were set up per reservoir by mixing 2 μl of protein solution (10 and 15 mg/ml in 10 mM Tris-HCl (pH 8.0), respectively) with 2 μl of reservoir solution.

For determination of the uncomplexed structure, single crystals were transferred to a harvesting buffer containing ammonium sulphate at 1.5-fold the concentration of the reservoir in 0.1 M Hepes buffer (pH 7.5). To soak XenA crystals with coumarin, 8-hydroxycoumarin and 7-hydroxycoumarin, crystals were cross-linked with 0.025% glutaraldehyde in harvesting buffer for 1 h, and then transferred to harvesting buffer containing 5 mM of the respective ligand and 5% DMSO for at least 30 min. The crystals belong to space group *I*222 with cell dimensions $a = 57.9$ Å, $b = 83.4$ Å, $c = 156.8$ Å, $\alpha = \beta = \gamma = 90°$ and contain one molecule per asymmetric unit. Visible absorption spectra of single XenA crystals were recorded using a micro spectrophotometer (4DXray Systems AB). The XenA crystals were mounted in a loop and kept at 100 K during absorption measurement.

The structure of XenA was determined by SIRAS phasing with a potassium iodide derivative, which is routinely being carried out with protein crystals of unknown structure. The derivative has been prepared by incubating the crystals for approximately 30 s in 400 mM potassium iodide dissolved in the harvesting buffer. The crystals were immediately frozen after soaking with iodide. Iodide sites were localized using SHELXD.[42,43] Initial phases were calculated using SHARP[44] (Table 2), and modified with SOLOMON.[45] To allow for automatic model building the modified experimental phases were combined with phases calculated from a positioned model of morphinone reductase (PDB-ID.: 1GWJ)[22] using AMoRe[46] for the Patterson search. The combined phases were further modified using the automatic building routine of wARP.[47] The model was built using MAIN 2000 [48], and atomic positions and *B*-factors were refined with CNS[49] (Table 3).

Protein Data Bank accession codes

The coordinates and structure factor amplitudes are deposited in the RCSB Protein Data Bank with ID codes: 2H8X, 2H8Z, and 2H90.

Acknowledgements

The authors thank Susanne Fetzner for donation of the *P. putida* 86 strain and helpful discussions, Juan Manuel Urbina-González and Ellen Wiedemann for assistance in the preparation of 8-hydroxycoumarin, Ilme Schlichting for the measurement of single crystal absorption spectra and Paul Roesch for access to the NMR facilities. R.P.J. is supported by a PhD fellowship of the Fonds der Chemischen Industrie. H.D. acknowledges the Deutsche Forschungsgemeinschaft (DO-785/2) for financial support.

References

1. Fetzner, S. (1998). Bacterial degradation of pyridine, indole, quinoline, and their derivatives under different redox conditions. *Appl. Microbiol. Biotecholn.* **49**, 237–250.
2. Fetzner, S., Tshisuaka, B., Lingens, F., Kappl, R. & Huttermann, J. (1998). Bacterial degradation of quinoline and derivatives - Pathways and their biocatalysts. *Ang. Chem.-Int. Ed.* **37**, 577–597.
3. Schwarz, G., Senghas, E., Erben, A., Schafer, B., Lingens, F. & Hoke, H. (1988). Microbial-metabolism of quinoline and related-compounds .1. Isolation and characterization of quinoline-degrading bacteria. *Syst. Appl. Microbiol.* **10**, 185–190.
4. Shukla, O. P. (1986). Microbial transformation of quinoline by a *Pseudomonas* sp. *Appl. Environ. Microbiol.* **51**, 1332–1342.
5. Blase, M., Bruntner, C., Tshisuaka, B., Fetzner, S. & Lingens, F. (1996). Cloning, expression, and sequence analysis of the three genes encoding quinoline 2-oxidoreductase, a molybdenum-containing hydroxylase from *Pseudomonas putida* 86. *J. Biol. Chem.* **271**, 23068–23079.
6. Kappl, R., Huttermann, J. & Fetzner, S. (2002). The molybdenum-containing hydroxylases of quinoline, isoquinoline, and quinaldine. *Met. Ions Biol. Syst.* **39**, 481–537.
7. Bonin, I., Martins, B. M., Purvanov, V., Fetzner, S.,

Huber, R. & Dobbek, H. (2004). Active site geometry and substrate recognition of the molybdenum hydroxylase quinoline 2-oxidoreductase. *Structure*, **12**, 1425–1435.
8. Rosche, B., Tshisuaka, B., Fetzner, S. & Lingens, F. (1995). 2-Oxo-1,2-dihydroquinoline 8-monooxygenase, a two-component enzyme system from *Pseudomonas putida* 86. *J. Biol. Chem.* **270**, 17836–17842.
9. Martins, B. M., Svetlitchnaia, T. & Dobbek, H. (2005). 2-Oxoquinoline 8-monooxygenase oxygenase component: active site modulation by Rieske-[2Fe-2S] center oxidation/reduction. *Structure*, **13**, 817–824.
10. Eicher, T. & Hauptmann, S. (2005). *The Chemistry of Heterocycles.* Wiley-VCH GmbH, Weinheim.
11. Fetzner, S. (2000). Enzymes involved in the aerobic bacterial degradation of N-heteroaromatic compounds: molybdenum hydroxylases and ring-opening 2,4-dioxygenases. *Naturwissenschaften*, **87**, 59–69.
12. Binks, P. R., French, C. E., Nicklin, S. & Bruce, N. C. (1996). Degradation of pentaerythritol tetranitrate by *Enterobacter cloacae* PB2. *Appl. Environ. Microbiol.* **62**, 1214–1219.
13. Fitzpatrick, T. B., Amrhein, N. & Macheroux, P. (2003). Characterization of YqjM, an Old Yellow Enzyme homolog from *Bacillus subtilis* involved in the oxidative stress response. *J. Biol. Chem.* **278**, 19891–19897.
14. Blehert, D. S., Knoke, K. L., Fox, B. G. & Chambliss, G. H. (1997). Regioselectivity of nitroglycerin denitration by flavoprotein nitroester reductases purified from two *Pseudomonas* species. *J. Bacteriol.* **179**, 6912–6920.
15. Snape, J. R., Walkley, N. A., Morby, A. P., Nicklin, S. & White, G. F. (1997). Purification, properties, and sequence of glycerol trinitrate reductase from *Agrobacterium radiobacter*. *J. Bacteriol.* **179**, 7796–7802.
16. Miura, K., Tomioka, Y., Suzuki, H., Yonezawa, M., Hishinuma, T. & Mizugaki, M. (1997). Molecular cloning of the nemA gene encoding N-ethylmaleimide reductase from *Escherichia coli*. *Biol. Pharm. Bull.* **20**, 110–112.
17. French, C. E. & Bruce, N. C. (1994). Purification and characterization of morphinone reductase from *Pseudomonas putida* M10. *Biochem. J.* **301**, 97–103.
18. Rohde, B. H., Schmid, R. & Ullrich, M. S. (1999). Thermoregulated expression and characterization of an NAD(P)H-dependent 2-cyclohexen-1-one reductase in the plant pathogenic bacterium *Pseudomonas syringae* pv. glycinea. *J. Bacteriol.* **181**, 814–822.
19. Kohli, R. M. & Massey, V. (1998). The oxidative half-reaction of Old Yellow Enzyme. The role of tyrosine 196. *J. Biol. Chem.* **273**, 32763–32770.
20. Blehert, D. S., Fox, B. G. & Chambliss, G. H. (1999). Cloning and sequence analysis of two *Pseudomonas* flavoprotein xenobiotic reductases. *J. Bacteriol.* **181**, 6254–6263.
21. Abramovitz, A. S. & Massey, V. (1976). Interaction of phenols with old yellow enzyme. Physical evidence for charge-transfer complexes. *J. Biol. Chem.* **251**, 5327–5336.
22. Barna, T., Messiha, H. L., Petosa, C., Bruce, N. C., Scrutton, N. S. & Moody, P. C. (2002). Crystal structure of bacterial morphinone reductase and properties of the C191A mutant enzyme. *J. Biol. Chem.* **277**, 30976–30983.
23. Fox, K. M. & Karplus, P. A. (1994). Old yellow enzyme at 2 A resolution: overall structure, ligand binding, and comparison with related flavoproteins. *Structure*, **2**, 1089–1105.
24. Kitzing, K., Fitzpatrick, T. B., Wilken, C., Sawa, J., Bourenkov, G. P., Macheroux, P. & Clausen, T. (2005). The 1.3 A crystal structure of the flavoprotein YqjM reveals a novel class of Old Yellow Enzymes. *J. Biol. Chem.* **280**, 27904–27913.
25. Holm, L. & Sander, C. (1993). Protein structure comparison by alignment of distance matrices. *J. Mol. Biol.* **233**, 123–138.
26. Xu, D., Kohli, R. M. & Massey, V. (1999). The role of threonine 37 in flavin reactivity of the old yellow enzyme. *Proc. Natl Acad. Sci. USA*, **96**, 3556–3561.
27. Barna, T. M., Khan, H., Bruce, N. C., Barsukov, I., Scrutton, N. S. & Moody, P. C. (2001). Crystal structure of pentaerythritol tetranitrate reductase: "flipped" binding geometries for steroid substrates in different redox states of the enzyme. *J. Mol. Biol.* **310**, 433–447.
28. Vaz, A. D., Chakraborty, S. & Massey, V. (1995). Old Yellow enzyme: aromatization of cyclic enones and the mechanism of a novel dismutation reaction. *Biochemistry*, **34**, 4246–4256.
29. Brown, B. J., Deng, Z., Karplus, P. A. & Massey, V. (1998). On the active site of Old Yellow Enzyme. Role of histidine 191 and asparagine 194. *J. Biol. Chem.* **273**, 32753–32762.
30. Khan, H., Barna, T., Bruce, N. C., Munro, A. W., Leys, D. & Scrutton, N. S. (2005). Proton transfer in the oxidative half-reaction of pentaerythritol tetranitrate reductase. Structure of the reduced enzyme-progesterone complex and the roles of residues Tyr186, His181, His184. *FEBS J.* **272**, 4660–4671.
31. Messiha, H. L., Bruce, N. C., Sattelle, B. M., Sutcliffe, M. J., Munro, A. W. & Scrutton, N. S. (2005). Role of active site residues and solvent in proton transfer and the modulation of flavin reduction potential in bacterial morphinone reductase. *J. Biol. Chem.* **280**, 27103–27110.
32. Race, P. R., Lovering, A. L., Green, R. M., Ossor, A., White, S. A., Searle, P. F. *et al.* (2005). Structural and mechanistic studies of *Escherichia coli* nitroreductase with the antibiotic nitrofurazone. Reversed binding orientations in different redox states of the enzyme. *J. Biol. Chem.* **280**, 13256–13264.
33. Cerqueira, N. M. F. S. A., Oliveira-Campos, A. M. F., Coelho, P. J., de Carvalho, L. H. M., Samat, A. & Guglielmetti, R. (2002). Synthesis of photochromic dyes based on annulated coumarin systems. *Helv. Chim. Acta*, **85**, 442–450.
34. Tshisuaka, B., Kappl, R., Huttermann, J. & Lingens, F. (1993). Quinoline oxidoreductase from *Pseudomonas putida* 86: an improved purification procedure and electron paramagnetic resonance spectroscopy. *Biochemistry*, **32**, 12928–12934.
35. Whitby, L. G. (1953). A new method for preparing flavin-adenine dinucleotide. *Biochem. J.* **54**, 437–442.
36. Hwang, T. L. & Shaka, A. J. (1995). Water suppression that works - excitation sculpting using arbitrary waveforms and pulsed-field gradients. *J. Magn. Reson. Ser. A*, **112**, 275–279.
37. Auchere, F., Bertho, G., Artaud, I., Girault, J. P. & Capeillere-Blandin, C. (2001). Purification and structure of the major product obtained by reaction of NADPH and NMNH with the myeloperoxidase/hydrogen peroxide/chloride system. *Eur. J. Biochem.* **268**, 2889–2895.
38. Miura, S. & Ichikawa, Y. (1994). Interaction of NADPH-adrenoferredoxin reductase with NADP+ and adrenoferredoxin. Equilibrium and dynamic properties investigated by proton nuclear magnetic resonance. *J. Biol. Chem.* **269**, 8001–8006.
39. Martinez-Martinez, F. J., Padilla-Martinez, I. I. & Trujillo-Ferrara, J. (2001). H-1 and C-13 NMR

assignments of 2-oxo-2H-1-benzopyran-3-acyl and-3-amide derivatives. *Magn. Reson. Chem.* **39**, 765–767.
40. Jeener, J., Meier, B. H., Bachmann, P. & Ernst, R. R. (1979). Investigation of exchange processes by 2-dimensional NMR-spectroscopy. *J. Chem. Phys.* **71**, 4546–4553.
41. Cobas, J. C. & Sardina, F. J. (2003). Nuclear magnetic resonance data processing. MestRe-C: a software package for desktop computers. *Concepts Magnetic Reson.* **19A**, 80–96.
42. Schneider, T. R. & Sheldrick, G. M. (2002). Substructure solution with SHELXD. *Acta Crystallog. sect. D*, **58**, 1772–1779.
43. Uson, I., Schmidt, B., von Bulow, R., Grimme, S., von Figura, K., Dauter, M. *et al.* (2003). Locating the anomalous scatterer substructures in halide and sulfur phasing. *Acta Crystallog. sect. D*, **59**, 57–66.
44. La Fortelle, E. D., Irwin, J. J. & Bricogne, G. (1997). SHARP: A maximum-likelihood heavy-atom parameter refinement and phasing program for the MIR and MAD methods. *Crystallog. Comput.* **7**, 1–9.
45. Collaborative Computational Project No. 4. (1994). The CCP4 Suite: programs for protein crystallography. *Acta Crystallog. sect. D*, **50**, 760–763.
46. Navaza, J. (1994). AMoRe: an automated package for molecular replacement. *Acta Crystallog. sect. A*, **50**, 157–163.
47. Perrakis, A., Sixma, T. K., Wilson, K. S. & Lamzin, V. S. (1997). wARP: Improvement and extension of crystallographic phases by weighted averaging of multiple-refined dummy atomic models. *Acta Crystallog. sect. D*, **53**, 448–455.
48. Turk, D. (1992). Weiterentwicklung eines Programms für Molekülgraphik und Elektronendichte-Manipulation und seine Anwendung auf verschiedene Protein-Strukturaufklärungen, TU München.
49. Brünger, A. T., Adams, P. D., Clore, G. M., Delano, W. L., Gros, P., Grosse Kunstleve, R. W. *et al.* (1998). Crystallography and NMR system: a new software suite for macromolecular structure determination. *Acta Crystallog. sect. D*, **54**, 905–921.
50. Laskowski, R. A., MacArthur, M. W., Moss, D. S. & Thornton, J. M. (1993). PROCHECK: a program to check the stereochemical quality of protein structures. *J. Appl. Crystallog.* **26**, 283–291.

Edited by R. Huber

(Received 4 April 2006; received in revised form 1 June 2006; accepted 7 June 2006)
Available online 21 June 2006